

PASSIVE SCALARS AND THREE-DIMENSIONAL LIOUVILLIAN MAPS *Julyan H.E. Cartwright^a, Mario Feingold^b and Oreste Piro^a

^a*Departament de Física, Universitat de les Illes Balears,
07071 Palma de Mallorca, Spain*

^b*Dept. of Physics, Ben-Gurion University,
Beer-Sheva 84105, Israel*

Abstract

Global aspects of the motion of passive scalars in time-dependent incompressible fluid flows are well described by volume-preserving (Liouvillian) three-dimensional maps. In this paper the possible invariant structures in Liouvillian maps and the two most interesting nearly-integrable cases are investigated. In addition, the fundamental role of invariant lines in organizing the dynamics of this type of system is exposed. Bifurcations involving the destruction of some invariant lines and tubes and the creation of new ones are described in detail.

Keywords: Incompressible fluid; passive scalars; three-dimensional volume-preserving maps; action-angle variables; invariant structures

Pacs: 05.45.+b

* Physica D, **76**, 22–33, 1994

1. Introduction

The dynamics of deterministic passive scalars suspended in incompressible fluid flows has very different characteristics as the dimensionality of the flow varies. In the most general formulation of the problem, we are interested the study of the trajectories given by the following set of differential equations:

$$\dot{\mathbf{r}} = \mathbf{u}(x, y, z, t), \quad (1)$$

where the velocity field $\mathbf{u}(x, y, z, t)$ satisfies

$$\nabla \cdot \mathbf{u} = 0. \quad (2)$$

Several simpler instances of the problem have been investigated thoroughly in the past decade.¹ Let us quickly review some of them.

When the flow is two-dimensional and stationary, Eq. (1) implies that the velocity field $\mathbf{u}(x, y)$ can be derived, from a *stream function* $\Psi(x, y)$

$$u_x = \frac{\partial \Psi}{\partial y} ; u_y = -\frac{\partial \Psi}{\partial x}. \quad (3)$$

In this case the equations of motion have a Hamiltonian structure with Ψ playing the role of the Hamiltonian. Hamiltonian systems with only one degree of freedom are always integrable. For bounded systems, this means that all the trajectories in the phase space are closed curves. Accordingly, trajectories of passive scalars in 2D steady flows will have the same topology.

Next in order of increasing complexity comes the class of time-periodic 2D flows.^{2–5} Here the stream function becomes time dependent and the system is equivalent to a non-autonomous Hamiltonian one. In this case, only integrable systems show a phase space completely foliated into invariant tori as in the previous case. However, the KAM theorem states that a measurable portion of these invariant tori persist in phase space even for finite departures from integrability. These invariant surfaces are relevant for passive scalar applications since they represent dynamical barriers for transport across space.

Steady 3D flows are somewhat equivalent to the case described in the previous paragraph. Arnold⁶ has shown that the motion of passive scalars in steady inviscid fluid flows

is integrable if $\omega = \nabla \times \mathbf{u}$ is almost nowhere parallel to \mathbf{u} . On the contrary, if the Beltrami condition $\omega = \lambda \mathbf{u}$ is satisfied, it has been found⁷ that trajectories which are chaotic coexist with regular ones. The regular trajectories cover two-dimensional surfaces which are invariant under the time evolution of the passive scalar. In turn, the invariant surfaces separate the available space into disconnected regions which confine the chaotic trajectories.

Next in complexity is the case of 3D flows with periodic time dependence. In this case, the form of the equations of motion is no longer Hamiltonian. However, the stroboscopic maps of such systems are three-dimensional and, by virtue of Eq. (2), volume preserving. In the following we will refer to these maps as 3D-Liouvillian⁸ or in short, 3DLM. The invariant structures displayed by these maps in the nearly integrable regime have been investigated in detail in the past^{9–13} because of their relevance to the mixing efficiency^{2,3} of fluid flows. In particular, we found one class of 3DLM where these structures divide the space into separate regions, preventing a single deterministic passive scalar trajectory from reaching the whole space. In another class of 3DLM, however, unbounded *deterministic* diffusion has been found arbitrarily near the corresponding integrable map.

We have also conjectured that the objects organizing the dynamics of 3DLMs are one dimensional quasiperiodic orbits which we name *invariant lines*. In this paper we review the former results and provide further evidence to support this picture.

Sec. 2 is devoted to the nearly-integrable behaviour of the 3DLM referred to above. In Sec. 3 we study the evolution of the structures related to invariant lines and tubes around them as the parameters of the maps are varied. We show that the disintegration of an invariant line into fixed points or periodic orbits at parameters values that make the line strongly resonant is accompanied by the birth of a new invariant line. The ubiquity of invariant lines is shown to follow from the generic topology of the invariant manifolds of the periodic orbits. Finally, in the concluding Sec. 4 we summarize our results and discuss some problems for future research.

2. Three-dimensional maps and their invariant structures

We concentrate our attention on volume-preserving maps $\mathbf{L} : \mathbf{T}^3 \rightarrow \mathbf{T}^3$ on the three-dimensional torus of the form

$$(x', y', z') = (x + u(y, z), y + v(x', z), z + w(x', y')), \quad (4)$$

where u , v , and w are doubly-periodic functions. In particular, we shall investigate the following truncation of the Fourier expansions for these functions:

$$\begin{aligned} x' &= x + A_1 \sin z + C_2 \cos y \pmod{2\pi}, \\ y' &= y + B_1 \sin x' + A_2 \cos z \pmod{2\pi}, \\ z' &= z + C_1 f(y') + B_2 g(x') \pmod{2\pi}, \end{aligned} \quad (5)$$

where the functions f and g are smooth on the circle.

In general we call *integrable* a map \mathbf{L}_k^0 for which a set of variables $\mathbf{I} \in \mathbf{R}^k$, $\theta \in \mathbf{T}^{3-k}$ can be found such that

$$\begin{aligned} \mathbf{I}' &= \mathbf{I}, \\ \theta' &= \theta + \omega(\mathbf{I}). \end{aligned} \quad (6)$$

Clearly, the variables \mathbf{I} , which we call *actions* by analogy with Hamiltonian dynamics, parametrize a family of $(3 - k)$ -dimensional geometrical objects that are invariant under the dynamics. In turn, the θ variables specify the position of a point on a given invariant object. At each iteration the angular variables rotate by an angle given by the corresponding component of the $(3 - k)$ -dimensional vector ω . This angle might in general vary from one invariant set to another, but remains constant for all the points on each of these sets. Let us describe the four possible cases:

(a) $k = 0$. Since there are no actions, the frequency vector ω is constant and this integrable case corresponds to a uniform rotation on T^3 .

(b) $k = 1$. The motion takes place on two-dimensional tori defined by $I = \text{const.}$ and a point on one of these tori is specified by the values of two angles θ_1, θ_2 . Therefore, the motion on these two-tori is a uniform rotation for which the frequency depends only on the value of the action.

(c) $k = 2$. In this case, there are two actions I_1, I_2 which parametrize a family of invariant circles (one-dimensional tori). The angular variable rotates with a frequency $\omega(I_1, I_2)$.

(d) $k = 3$. In this case, the map in Eq. (6) is the identity and each point of the space (parametrized by I_1, I_2 and I_3) is invariant. There are no angles in this problem.

For case (a) the results of Ruelle and Takens^{14,15} indicate that small perturbations of the integrable system will produce completely chaotic maps. Although the implication of volume preservation for these results is a very interesting problem, it lies outside the scope of this work, which aims towards the understanding of lower-dimensional invariant objects. At the opposite extreme, $k = 3$, the nearly integrable systems are small perturbations of the identity $\mathbf{I}' = \mathbf{I} + \epsilon\mathbf{F}(\mathbf{I})$ or $\Delta\mathbf{I} = \epsilon\mathbf{F}(\mathbf{I})$. In the $\epsilon \rightarrow 0$ limit, the dynamics of this system can be described by a set of three autonomous differential equations after an appropriate rescaling of the time. This case (d) also lies outside the interest of the present paper. Therefore, we shall consider only small perturbations \mathbf{L}_1 and \mathbf{L}_2 around the respective integrable maps \mathbf{L}_1^0 and \mathbf{L}_2^0 .

An example of nearly-integrable maps with a single action is the map \mathbf{L}_1 given by the following restriction of Eq. (5):

$$\begin{aligned} x' &= x + A \sin z + \epsilon\alpha_C \cos y \\ y' &= y + \epsilon\alpha_B \sin x + A \cos z \\ z' &= z + \epsilon\alpha_C \sin y' + \epsilon\alpha_B \cos x'. \end{aligned} \tag{7}$$

At $\epsilon = 0$ this map is integrable with only one action variable z . The motion in this limit takes place on the surfaces of constant z , and the angular variables x and y rotate at each iteration by constant angles $\omega_x = A \sin z$ and $\omega_y = A \cos z$ respectively. The map in Eq. (7) corresponds to a discretization of the ABC model proposed by Arnold⁶ as an example of chaotic streamlines in a stationary 3-dimensional flow, and extensively studied by Dombre et al.⁷ The discretization is equivalent to the addition of periodic time dependence to the flow.

In order to investigate the effect of a small nonintegrable perturbation of amplitude ϵ on the form of the invariant surfaces, we implement a perturbative scheme. The condition for a surface defined by the equation $\mathbf{r} = \mathbf{r}(t, s)$ (where $\mathbf{r} = (x, y, z)$ and t, s are parameters)

to be invariant is

$$\mathbf{L}_1(\mathbf{r}(t, s)) = \mathbf{r}(t', s'). \quad (8)$$

We start with the invariant surface $z = z_0$ of the integrable case and suppose that the perturbed surface can be written in the form $z = z_0 + \sum \epsilon^n H_n(x, y)$. Here the parameters t and s are identified with the coordinates x and y . Inserting this expression into the invariance condition, we obtain an infinite system of linear functional equations for the unknown functions H_n that in principle can be solved order by order. The first step in this expansion leads to

$$\begin{aligned} z' &= z_0 + \epsilon H_1(x', y') + O(\epsilon^2) = z_0 + \epsilon H_1(x + A \sin z_0, y + A \cos z_0) + O(\epsilon^2) \\ &= z_0 + \epsilon H_1(x, y) + \epsilon \alpha_C \sin(y + A \cos z_0) + \epsilon \alpha_B \cos(x + A \sin z_0) + O(\epsilon^2). \end{aligned} \quad (9)$$

Consequently, $H_1(x, y)$ satisfies the linear functional equation

$$H_1(x + A \sin z_0, y + A \cos z_0) = H_1(x, y) + \alpha_C \sin(y + A \cos z_0) + \alpha_B \cos(x + A \sin z_0). \quad (10)$$

The previous equation can be easily solved by expanding $H_1(x, y)$ in a double Fourier series. Setting $H_1(x, y) = \sum a_{mn} e^{i(mx+ny)}$ in (10) we obtain

$$\begin{aligned} a_{mn} [e^{i(mA \sin z_0 + nA \cos z_0)} - 1] &= i \frac{\alpha_C}{2} [\delta_{-1,n} e^{-iA \cos z_0} - \delta_{1,n} e^{iA \cos z_0}] \delta_{0,m} \\ &\quad + \frac{\alpha_B}{2} [\delta_{1,m} e^{iA \sin z_0} + \delta_{-1,m} e^{-iA \sin z_0}] \delta_{0,n}. \end{aligned} \quad (11)$$

Notice that the coefficients a_{mn} in Eq. (11) remain undefined if the resonance condition

$$mA \sin z_0 + nA \cos z_0 = 2\pi k \quad (12)$$

is satisfied for $(m, n, k) = (\pm 1, 0, k), (0, \pm 1, k)$. However, they can be uniquely determined by requiring that a_{mn} -s be continuous functions of z . Thus, the only four non-zero coefficients in $H_1(x, y)$ are $a_{0,\pm 1}$ and $a_{\pm 1,0}$. This is, however, a peculiarity emerging from the form of the nonlinear terms in the equation for the action z . If higher-order Fourier components were considered in the original map, then more non-zero coefficients would appear in the expression for H_1 . Also, in our case, when the expansion is carried over to higher orders in ϵ , the corrections H_n will contain correspondingly-higher-order Fourier coefficients.

Eq. (12) has stronger consequences when it holds for $(m, n, k) = (\pm 1, 0, k)$ and $(m, n, k) = (0, \pm 1, k)$. Namely, the values of $a_{0, \pm 1}$ and $a_{\pm 1, 0}$ respectively are diverging. This occurs, of course, only for few special values of z_0 . The invariant surfaces where the condition (12) is satisfied, are called *resonant*. It is clear from the perturbative arguments that these resonant surfaces will exhibit a strongly-singular behaviour at finite ϵ . To understand this special behaviour notice first that integrable motion on a resonant surface is such that each individual trajectory is not dense on the surface but rather fills an invariant curve contained in it. For $\epsilon = 0$ there is a continuous family of such invariant lines covering the entire surface. At $\epsilon \neq 0$ however, only a finite (and even) number of such lines survives the presence of the nonlinear perturbation. This occurs by a mechanism similar to the Poincaré–Birkhoff phenomenon for periodic orbits in 2D. Moreover, as in the latter case, it turns out that half of these lines are stable (elliptic) and the other half, unstable (hyperbolic). In the next section we will illustrate the origin of such behaviour with a perturbative calculation. At non-zero perturbation strength ϵ a family of elliptic invariant tubes is formed around the stable lines. Similarly, associated with the unstable lines an H-shaped chaotic slab emerges. This scheme is repeated for higher-order resonances at the corresponding order of the perturbation expansion.

For the surfaces where the frequencies ω are far from satisfying the resonance condition, we might expect that some version of the KAM theorem will hold and that slightly-deformed invariant surfaces will persist if ϵ is not too big. Actually, there is extensive numerical evidence in favour of such a conjecture. In Fig. 1, the various types of trajectories are shown for the map of Eq. (7).

By comparing this picture with the analogous one for 2D-Hamiltonian systems, one is tempted to conjecture that the organizing role played by the periodic orbits in the latter should be assigned here to the invariant lines. In fact, in the same way that invariant tori of the 2D case can be systematically approached with sequences of periodic orbits, in our case a similar (but unfortunately not so systematic) approximating strategy can be designed by using invariant lines instead. In Sec. 3, we will see that one-dimensional invariant objects pervade the phase space of these systems and their presence seems to be a robust property.

The reader can easily recognize that the preserved invariant surfaces are barriers through which a chaotically moving particle cannot penetrate. In other words, diffusion of an individual trajectory throughout the entire space is not allowed. We will show, however,

that the opposite holds for \mathbf{L}_2 maps.

Let us now consider the maps close to the integrable case with two almost-conserved quantities, \mathbf{L}_2 :

$$\begin{aligned} I'_1 &= I_1 + \epsilon P_1(I_2, \theta) ; I'_2 = I_2 + \epsilon P_2(I'_1, \theta) \\ \theta' &= \theta + \omega(I'_1, I'_2). \end{aligned} \quad (13)$$

At $\epsilon = 0$ the motion takes place on lines $\mathbf{I} = (I_1, I_2) = \text{const.}$ We could examine the perturbative behaviour of those invariant lines with the hope of finding some sort of KAM result for them. However, by a mechanism similar to the one responsible for breaking the resonant surfaces in \mathbf{L}_1 maps, all the invariant lines are destroyed to first order in ϵ . Later, we shall illustrate this process with a particular example. In fact, we can understand the origin of the singularity of this integrable case by means of the following argument based on an adiabatic approximation. Suppose that $\omega(\mathbf{I})$ is irrational for some given values of the arguments. In the limit of $\epsilon \rightarrow 0$, we can assume that before \mathbf{I} changes significantly, the angle θ covers uniformly the entire $(0, 2\pi)$ interval. Under these circumstances, the variation of \mathbf{I} can only be sensitive to averages of $\mathbf{P} = (P_1, P_2)$ over all the possible values of θ . Therefore

$$\Delta \mathbf{I} = \epsilon \langle \mathbf{P}(\mathbf{I}, \theta) \rangle_\theta = \epsilon \bar{\mathbf{P}}(\mathbf{I}) \quad (14)$$

where $\langle \rangle_\theta$ stands for the θ -average. Thus, the dynamics of the action variables decouples from θ for non-resonant ω . Eq. (14) leads in the limit $\epsilon \rightarrow 0$ to a system of two ordinary differential equations

$$\frac{d\mathbf{I}}{dt} = \bar{\mathbf{P}}(\mathbf{I}) \quad (15)$$

where the identification $\epsilon = \Delta t$ was made. This system can be easily integrated by variable separation. Its trajectories $\mathbf{I}(t)$ satisfy

$$\int_0^{I_2} \bar{P}_1(I) dI - \int_0^{I_1} \bar{P}_2(I) dI = W(I_1, I_2) = \text{const.} \quad (16)$$

In other words, in the $\epsilon \rightarrow 0$ limit, the action variables slowly evolve along the curves defined by Eq. (16). Including the fast motion in the θ direction, we infer that the originally-invariant lines parallel to the θ axis coalesce in invariant surfaces Σ_β defined by the condition $W(I_1, I_2) = \beta$. A typical trajectory will densely cover such surfaces rather than move on

an invariant curve. The adiabatic approximation is exact in the limit $\epsilon \rightarrow 0$. One is then tempted to conclude that the situation is similar to the one described for one-action maps in the sense that the adiabatic invariant surfaces can survive when finite nonlinearities are present. However, a new and very interesting phenomenon appears in \mathbf{L}_2 maps. We first notice that the adiabatic approximation is bound to fail whenever the resonance condition $\omega(I_1, I_2) = 2\pi k/n$ is satisfied. Moreover, this condition defines a family of surfaces which in a generic case does not coincide with the family of invariant surfaces. As a consequence, each invariant surface will intersect at least one resonance sheet. At the intersections, the adiabatic approximation is spoiled and so is the smoothness of the invariant surfaces. Far from the intersection, however, one expects that trajectories evolve on surfaces which are slight deformations of the ones given by Eq. (16). In order to exemplify the characteristic behaviour of \mathbf{L}_2 maps, we use an appropriate restriction of the family of maps defined in Eq. (5):

$$\begin{aligned} x' &= x + \epsilon\alpha_{A_1} \sin z + \epsilon\alpha_{C_2} \cos y \\ y' &= y + \epsilon\alpha_{B_1} \sin x' + \epsilon\alpha_{A_2} \cos z \\ z' &= z + C_1 f(y') + B_2 g(x'). \end{aligned} \tag{17}$$

For $\epsilon = 0$, the map in Eq (17) is integrable and has the form of Eq. (13). In this case the lines corresponding to constant values of x and y are invariant. A search for invariant lines of the form $(x, y) = (x_0, y_0) + \sum (X_n(z), Y_n(z))\epsilon^n$, in the nearly-integrable case can be performed perturbatively. The order- ϵ calculation leads to the following couple of functional equations

$$X[z + C_1 f(y_0) + B_2 g(x_0)] = X(z) + \alpha_{A_1} \sin z + \alpha_{C_2} \cos y_0, \tag{18a}$$

$$Y[z + C_1 f(y_0) + B_2 g(x_0)] = Y(z) + \alpha_{B_1} \sin x_0 + \alpha_{A_2} \cos z. \tag{18b}$$

Clearly, the constant terms containing x_0 and y_0 in Eq. (18) lead to the divergence of the zeroth-order Fourier coefficient of the $X(z)$ and $Y(z)$ functions. Since $\langle \sin z \rangle_z = \langle \cos z \rangle_z = 0$, the adiabatic invariant surfaces Σ_β of Eq. (16) become

$$W_0(x, y) = \alpha_{C_2} \sin y + \alpha_{B_1} \cos x = \beta. \tag{19}$$

Fig. 2 shows some of these surfaces projected down to the $z = 0$ plane. To illustrate the effect of the resonances, we plot in Fig. 3 a trajectory of the map in Eq. (17) for a non-zero but very small value of ϵ . The location of the lowest-order resonance $\omega = 0$ for a particular election of the functions f and g is indicated by the dashed line. Close to this line, the trajectory oscillates wildly and jumps from one adiabatic surface to another.

To depict this behaviour in a different way, we show in Fig. 4 the time evolution of the value of W_0 , which would be constant if the adiabatic approximation were exact. One can easily recognize intervals where W_0 is almost constant followed by relatively short periods of oscillatory behaviour. Naturally, these oscillations occur whenever the trajectory crosses the first-order resonance. Notice that as a consequence of these oscillations, W_0 randomly jumps from one asymptotically-constant value to another, corresponding to two different adiabatic surfaces.

One striking consequence of this dynamical behaviour is that a single trajectory can in principle visit the entire region of space where the adiabatic surfaces which intersect with the first-order resonance reside. The size of this region can be controlled by choosing the functional form of the frequency ω . In Fig. 5. we show two nearly-extreme cases. In the first one (Fig. 5a), a case where the resonance condition almost coincides with one of the adiabatic invariant surfaces is shown. Several initial conditions have been used to generate this picture. Notice that most of the trajectories evolve on smooth surfaces which are roughly the same as those shown in Fig. 2. In addition, one can observe a small region of chaotic trajectories associated with the invariant surfaces intersecting the first-order resonance condition. Of course, higher-order resonances have similar effects in other regions of the space, but these are not evident on the time scale of the picture. On the other hand, Fig. 5b shows the opposite extreme. Here, the first-order resonance indicated by the dashed line intersects almost all the surfaces of Eq. (19). In this figure, the iterations of only one trajectory are shown. It is now apparent that this single trajectory visits all the available space. The rate of diffusion, D , has been estimated analytically in Ref. 12. For the case of Fig. 5b it is shown that $D = O(\epsilon^2)$. Numerically, we found that $D = O(\epsilon^\gamma)$ where $\gamma = 2.0 \pm 0.3$.

3. Tubes and invariant lines

The standard approach to the systematic study of maps and their properties is based on the principle of decomposition in terms of the simplest type of invariant objects. Since in 3DLM, periodic orbits are generically unstable,¹⁰ the lowest-order invariant objects which underlie the organization of the dynamics are the invariant lines. In the case of \mathbf{L}_1 maps, invariant lines behave in a way which is reminiscent of the fixed points in 2D conservative maps. In particular, slices through the dynamics on the (x, y, z) -torus transversal to one of the angle directions, x or y , are similar to phase-space portraits of the standard map for example.¹⁰ To some extent however, this similarity is misleading. It gives the wrong impression that a simple extrapolation to one more dimensions of the theory for periodic orbits is sufficient for the understanding of invariant lines in 3DLM. In fact, while periodic orbits are solutions of *algebraic* equations, in order to find invariant lines one has to solve *functional* equations. In this section, we shall illustrate this difference through the study of the simplest *bifurcations* which the invariant lines undergo. By analogy with the case of periodic orbits, bifurcations are qualitative changes in the properties of invariant lines occurring as the parameters of the map vary. In what follows, we restrict ourselves to bifurcations in which invariant lines are either created or destroyed.

The simplest and most dramatic destruction of invariant lines occurs when the non-integrability parameter, ϵ , is turned on. As described in Sec. 2, the continuous families of invariant lines present in the integrable case are replaced with a few stable tubes and a chaotic slab (see Fig. 1). To illustrate this process we can implement a perturbative scheme for invariant lines which is similar to the one already used for surfaces. For the sake of clarity we restrict ourselves to the $(\pm 1, 0, 0)$ resonant surfaces. In the integrable case this resonance occurs if $\omega_x = A \sin z_0 = 0$ i.e., at $z_0 = z_i$ with $z_1 = 0$ and $z_2 = \pi$. It is clear that the trajectories on these resonant surfaces lie on lines parallel to the y -axis. Each initial condition x_0 on the resonant surface corresponds to a different line which is consequently defined by $x = x_0$ and $z = z_i$. We want to understand what happens with these lines when $\epsilon \neq 0$. Therefore, we will look for perturbed lines of the form

$$x = x_0 + \epsilon X(y) + O(\epsilon^2) \quad ; \quad z = z_i + \epsilon Z(y) + O(\epsilon^2) \quad (20)$$

and confine our calculations to order ϵ . By requiring invariance of (20) under the iteration

of the map, we find two functional equations, for $X(y)$ and $Z(y)$

$$X(y + A \cos z_i) = X(y) + AZ(y) \cos z_i + \cos y, \quad (21a)$$

$$Z(y + A \cos z_i) = Z(y) + \sin(y + A \cos z_i) + \alpha_B \cos x_0. \quad (21b)$$

As before, expanding the two functions in Fourier series, $X(y) = \sum a_n^x e^{iny}$ and $Z(y) = \sum a_n^z e^{iny}$ we obtain for the coefficients

$$a_n^x (e^{inA \cos z_i} - 1) = A \cos z_i a_n^z + \frac{1}{2}(\delta_{1,n} + \delta_{-1,n}), \quad (22a)$$

$$a_n^z (e^{inA \cos z_i} - 1) = \frac{i}{2}[\delta_{-1,n} e^{-iA \cos z_i} - \delta_{1,n} e^{iA \cos z_i}] + \delta_{0,n} \alpha_B \cos x_0. \quad (22b)$$

Notice that when $n = 0$, the factor $(e^{inA \cos z_i} - 1)$ vanishes whereas the r.h.s of Eq. (22b) does not. Therefore, the first order correction for the invariant lines is finite only if $\cos x_0 = 0$. This implies that out of the infinity of invariant lines corresponding to the $(\pm 1, 0, 0)$ resonant surfaces $z_0 = z_i$, only those defined by the (x_0, z_i) pairs $(\pi/2, \pi)$, $(3\pi/2, 0)$, $(\pi/2, 0)$ and $(3\pi/2, \pi)$ survive at first order in ϵ . Numerical computations indicate that half of these lines are dynamically stable and the other half are unstable. This result is a remarkable manifestation in 3DLM of a scenario similar to the one which, for Hamiltonian systems, is predicted by the Poincaré-Birkhoff theorem.¹⁶ While around stable lines, a family of elliptic invariant tubes is formed, associated with the unstable lines an H-shaped chaotic slab emerges. This scheme is repeated for higher-order resonances at the corresponding order of the perturbation expansion. The location of the lowest-order elliptic lines is indicated schematically in Fig. 6.

A different bifurcation, in which tubes are created rather than destroyed, takes place at $A = 2\pi$. For $A \geq 2\pi$, one has additional $O(\epsilon)$ solutions to the invariant-surface resonance condition of Eq. (12) of the type $(m, n, k) = (\pm 1, 0, \pm 1)$ and $(m, n, k) = (0, \pm 1, \pm 1)$. As before, these solutions correspond to elliptic tubes embedded in a chaotic slab. Since all the new tubes have similar properties, we only consider the $(0, \pm 1, \pm 1)$ ones. For these tubes, $\omega_x = \pm \sqrt{A^2 - 4\pi^2}$, $\omega_y = 2\pi$ for all values of A , and therefore, for $A > 2\pi$, they are parallel to the x -axis. Their average position in z , z_i , satisfies $\cos z_i = \pm 2\pi A^{-1}$. Unlike the tubes of Fig. 6, the new tubes travel along the z -direction as the parameter A changes. Accordingly, we shall refer to them as *travelling tubes*. At $A = 2\pi$, the

travelling tubes are created at $z_i = 0, \pi$, at apparently the same position at which the old $(\pm 1, 0, 0)$ -tubes lie in the perpendicular direction. One would naively expect that the collision between the new and the old tubes would lead to an increase in the degree of chaos in this part of space. While numerical investigations¹⁰ do indeed confirm this expectation, it turns out that the actual scenario is more subtle. In fact, at $A = 2\pi$, the $(\pm 1, 0, 0)$ invariant lines themselves become resonant (see Eq. (22)). This is simply a manifestation of the fact that at $\epsilon = 0$, each of these lines is a continuous family of *fixed points* with $\omega_y = 2\pi$. Accordingly, at finite ϵ , the corresponding tubes degenerate into chaotic trajectories in a range of $O(\sqrt{\epsilon})$ around $A = 2\pi$. Remarkably, it is within this range that the *travelling tubes* are born. These appear as regular trajectories which glue together pairs of fixed points of the type $(\omega_x, \omega_y, \omega_z) = (0, 2\pi, 0)$. Such fixed points exist in the interval $A \in (2\pi - \epsilon\alpha_B\alpha_C, 2\pi + \epsilon\alpha_B\alpha_C)$ at (x_0, y_0, z_0) such that, to lowest order in ϵ and with $\delta \equiv A - 2\pi$

$$\begin{aligned} \cos x_0 &= \pm \sqrt{1 - \frac{\delta^2}{\epsilon^2 \alpha_B^2 \alpha_C^2}} ; \quad \cos y_0 = \pm \sqrt{1 - \alpha_B^2 - \frac{\delta^2}{\epsilon^2 \alpha_C^2}}, \\ \sin z_0 &= \pm \frac{1}{2\pi} \sqrt{\epsilon^2 \alpha_C^2 (1 - \alpha_B^2) + \delta^2}. \end{aligned} \quad (23)$$

The \pm signs in Eq. (23) are restricted such that only eight fixed points are obtained which, at the lower end of the existence interval, are pairwise degenerate. Here, the pairs lie at $(\frac{\pi}{2}, 0, \pi)$, $(\frac{\pi}{2}, \pi, \pi)$, $(\frac{3\pi}{2}, 0, 0)$ and $(\frac{3\pi}{2}, \pi, 0)$. For $A > 2\pi - \epsilon\alpha_B\alpha_C$ this degeneracy is lifted and the fixed points belonging to a pair drift away from each other mainly in the x -direction. For example, at $A = 2\pi$ the members of each pair are two quadrants apart in x . Moreover, at the upper end of the existence interval, the fixed points in each pair collide after having wrapped once around the x -direction.

We now turn to discussing the properties of trajectories that lie in the vicinity of the fixed points. For this, one needs to understand the behaviour of the corresponding stable and unstable manifolds. The fixed points in each pair have two complex-conjugate eigenvalues and one real. While, for one of the fixed points, the complex eigenvalues correspond to a 2D-stable manifold and the real eigenvalue to a 1D-unstable manifold, for the second fixed point it is the other way around. Moreover, when A is just slightly larger than $2\pi - \epsilon\alpha_B\alpha_C$, the manifolds corresponding to the real eigenvalue are directed towards the second fixed

point of the pair. However, generically the two 1D manifolds do not meet but rather wind up around each other approximately filling up a tube which runs between the two fixed points and then opens up along the complex manifolds. This structure of the manifolds generates a region of chaotic motion that can be considered as the generalization of Shilnikov chaos to 3D maps.¹⁷ Remarkably, this scenario parallels the one in 2D Hamiltonian maps. Notice however that while in 2D the intersections of the manifolds are unavoidable, in 3D such intersections are non-generic. The parallelism between the two can instructively be pursued further. In the same way as in 2D, the heteroclinic chaotic regions are usually bounded by regular quasiperiodic motion on invariant curves encircling the elliptic periodic orbits; in our 3D example, the Shilnikov-type chaos is bounded by a nested family of toroidal surfaces, each hosting three-frequency quasiperiodic motion. Through the interior of this family runs a circular invariant line (which comes as a replacement for the elliptic point in the 2D picture) and it is threaded by both the stable/unstable manifold pair of the fixed points and their associated Shilnikov-chaotic trajectories. A trajectory lying on one of these doughnut-shaped surfaces is shown in Fig. 7.

As the fixed points move apart, they pull the tori along, stretching them into *travelling tubes* by the time they collide on the other side of the x -circle (see Fig. 8). One expects similar bifurcations leading to new *travelling tubes* to take place for all $A = 2\pi l$ with $l = 1, 2, \dots$. Therefore, at large enough A , space will be mostly filled with such tubes rather than with invariant surfaces as is the case for $A < 2\pi$.

4. Concluding remarks

Three-dimensional Liouvillian maps present an extremely rich variety of dynamical phenomena. Many of these phenomena show an analogy in the nearly-integrable limit to the behaviour of Hamiltonian systems of either two or three degrees of freedom, which generate symplectic maps in two and four dimensions respectively. The similarity with one or the other is governed by the number of invariant quantities of the corresponding integrable system.

Recent progress has been made in the direction of extending KAM results to this kind of dynamical system. However, there are several interesting problems which are still open and whose solutions, although probably relying on straightforward extensions

of the approaches used in other dynamical systems, require the development of non-trivial techniques. For example, in the case of maps with one action, the smooth two-dimensional KAM surfaces break at a critical value of the nonlinearity parameter. The question of how these surfaces behave at the breakdown point arises as a natural extension of similar studies in two-dimensional area-preserving maps. In our context, however, the problem becomes a version of the still-unsolved transition to chaos in three-frequency systems. Our studies strongly suggest that its solution requires the ability to investigate the invariant lines playing the role of periodic orbits in the lower-dimensional case. In fact, we have shown in Sec. 3 that the appearance of these objects is generic even in the parameter regions where the, in this case more elusive, periodic orbits are present.

The ergodic properties of L_2 maps should be extensively investigated. We were able to obtain good estimates for the diffusion rate in the regions dominated by the first-order resonances. However, one can imagine a situation where a fraction of the adiabatic surfaces do not cross any first-order resonance. In these regions the local diffusion rate is determined by the resonances with $n \geq 2$. A better understanding of the interaction between the adiabatic and resonant motions is required to obtain a similarly-reliable estimate for this case.

Finally, it is important to remark that the codimension of the whole class of Liouvillian-maps is higher than that of the families that we have studied. Therefore, it is very relevant to applications in hydrodynamics to investigate (a) the conditions for which real 3D time-periodic flows approach the subclass presented here, and (b) to what extent the reported behaviour extends beyond the limits of such a subclass. Research in these directions is currently in progress.

Acknowledgements

We thank K. Bajer, U. Frisch, L. P. Kadanoff, E. Moses, Y. Pomeau, I. Procaccia, E. Spiegel, M. Tabor and A. Vulpiani for useful discussions. This work has been supported in part by NSF-DMR under grant number 85-19460. M.F. acknowledges the support of an Allon Fellowship and O.P. and J.H.E.C. that of Dirección General de Investigación Científica y Técnica, contract number PB92-0046-c02-02 and EEC Human Capital and Mobility contract number ERBCHBICT920200.

References

1. J.M. Ottino, *The Kinematics of Mixing*, (Cambridge University Press, Cambridge, 1989); A. Crisanti, M. Falcioni, G. Paladin, and A. Vulpiani, Riv. Nuovo Cimento **14** (1991) 1.
2. H. Aref, J. Fluid Mech. **143** (1984) 1.
3. W. L. Chien, H. Rising, and J. M. Ottino, J. Fluid Mech. **170**, (1986) 355.
4. J. Chaiken, R. Chevray, M. Tabor, and Q. M. Tan, Proc. R. Soc. A **408** (1986) 165.
5. T. H. Solomon, and J. P. Gollub, Proceedings of the Fritz Haber International Symposium, Ed. I. Procaccia, (Plenum, New York, 1987).
6. V. I. Arnold, C. R. Acad. Sci. Paris **261** (1965) 17.
7. T. Dombre, U. Frish, J. M. Green, M. Henon, A. Mehr, and A. M. Soward, J. Fluid Mech. **167** (1986) 353.
8. E. Spiegel, private communication.
9. M. Feingold, L. Kadanoff and O. Piro, in *Fractal Aspects of Materials: Disordered Systems*, Eds. A.J. Hurd, D.A. Weitz and B.B. Mandelbrot (Materials Research Society, Pittsburgh, 1987).
10. M. Feingold, L. P. Kadanoff, and O. Piro, J. Stat. Phys. **50** (1988) 529.
11. M. Feingold, L. P. Kadanoff and O. Piro, in *Universalities in Condensed Matter*, Eds. R. Jullien, L. Peliti, R. Rammal and N. Boccara, Springer Proc. Phys. (Springer, Berlin, Heidelberg, 1988).
12. O. Piro and M. Feingold, Phys. Rev. Lett. **61** (1988) 1799.
13. M. Feingold, L.P. Kadanoff and O. Piro, in *Instabilities and Nonequilibrium Structures*, eds. E. Tirapegui and D. Villarroel (D. Reidel, Dordrecht, 1989).
14. D. Ruelle, and F. Takens, Comm. Math. Phys. **20** (1971) 167.
15. S. Newhouse, D. Ruelle, and F. Takens, Comm. Math. Phys. **64** (1978) 35.
16. A. J. Lichtenberg, and M. A. Liberman, *Regular and Stochastic Motion*, (Springer Verlag, New York, 1983).
17. This phenomenon has been studied by V. Rom-Kedar, L.P. Kadanoff, E.S.C. Ching, and C. Amick (Physica D **62** (1992) 51) in the context of maps of the type L_3 . However,

we found that a similar structure appears in the vicinity of the fixed points of \mathbf{L}_1 maps satisfying a strong resonance condition. The relation becomes clear after one realizes that the \mathbf{L}_1 maps are locally of \mathbf{L}_3 type in these regions.

Figure Captions

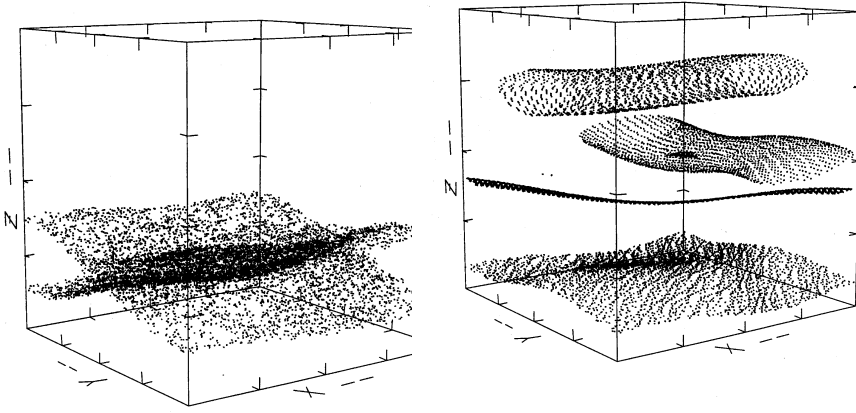


Fig. 1. Numerically obtained invariant surfaces and chaotic volumes. The parameter values in Eq. (7) are $A = 1.5$, $\alpha_B = 1$, $\alpha_C = 2$ and $\epsilon = 0.1$. (a) In order of increasing z : non-resonant surface ($x_0 = 0$, $y_0 = 0.56$, $z_0 = 0.11$) and tubular surfaces around the $(1, -1, 0)$, $(1, 0, 0)$ and $(0, 1, 0)$ resonances $-(x_0 = 0$, $y_0 = 0.9$, $z_0 = 0.395)$, $(x_0 = 0.75$, $y_0 = 0$, $z_0 = 0.4626)$ and $(x_0 = 0$, $y_0 = 0.5$, $z_0 = 0.828)$ respectively. (b) H-shaped chaotic volume associated with the *hyperbolic* line of the $(0, 1, 0)$ resonance ($x_0 = 0$, $y_0 = 0.5$ and $z_0 = 0.24$). All the initial conditions are indicated in fractions of 2π and the box represents the $[0, 2\pi]^3$ region.

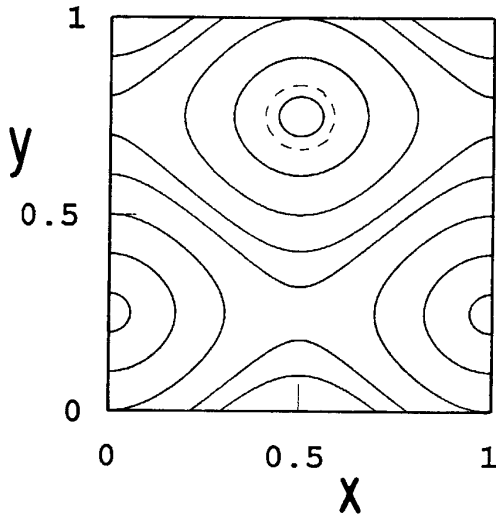


Fig. 2. A few members of the family of surfaces defined by Eq. (17) for $\alpha_{B_1} = 1.5$ and $\alpha_{C_2} = 2$ projected down to the $z = 0$ plane. For comparison, the dashed curve is the first turn of the trajectory depicted in Fig. 3.

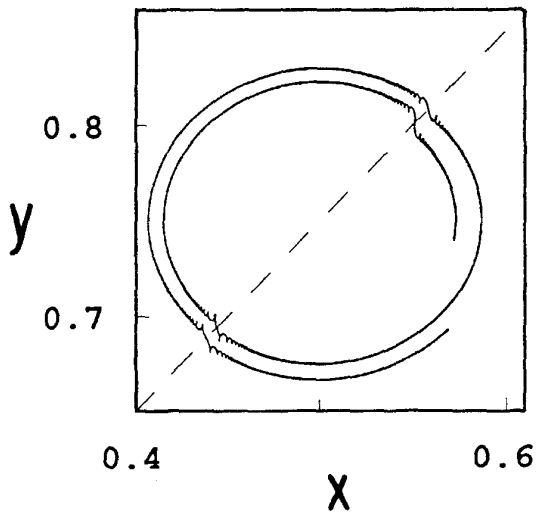


Fig. 3. One trajectory of the map in Eq. (17) for $\alpha_{A_1} = 1$, $\alpha_{A_2} = 2.5$, $C_1 = B_2 = 4$ and $\epsilon = 0.001$, $f = \cos$ and $g = \sin$. α_{B_1} and α_{C_2} are the same as in Fig. 2. The dashed line indicates the location of the lowest-order resonance.

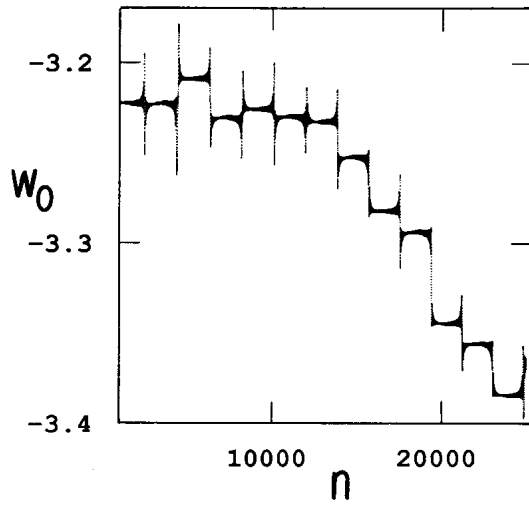


Fig. 4. $W_0(x_n, y_n)$ (Eq (19)) vs. n . The map and parameter values are the same as in Fig. 3.

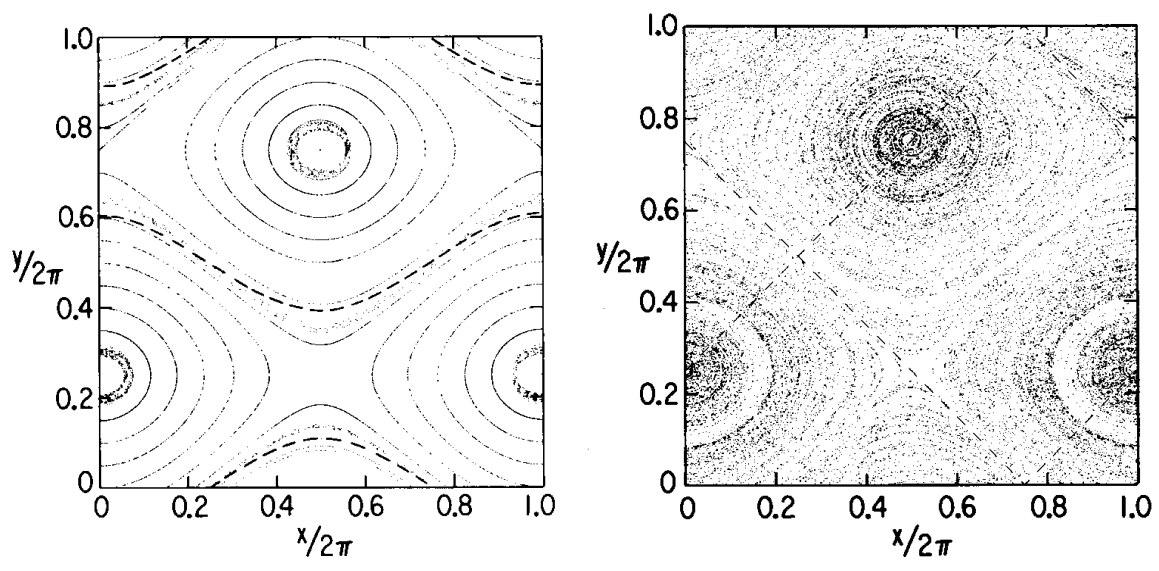


Fig. 5. Iterations of the map in Eq. (17) lying in the slice $0 \leq z \leq 0.01$. The dashed lines indicate the location of the lowest-order resonances. (a) $C_1 = 2.5$, $B_2 = 4$, $f = \sin$, $g = \cos$ and the remaining parameters are as in Fig. 4. Several initial conditions distributed along the y -axis and the $x = \pi$ line were necessary to obtain this picture. (b) f , g and all the parameters are the same as in Fig. 3. Only one initial condition is required to generate this picture.

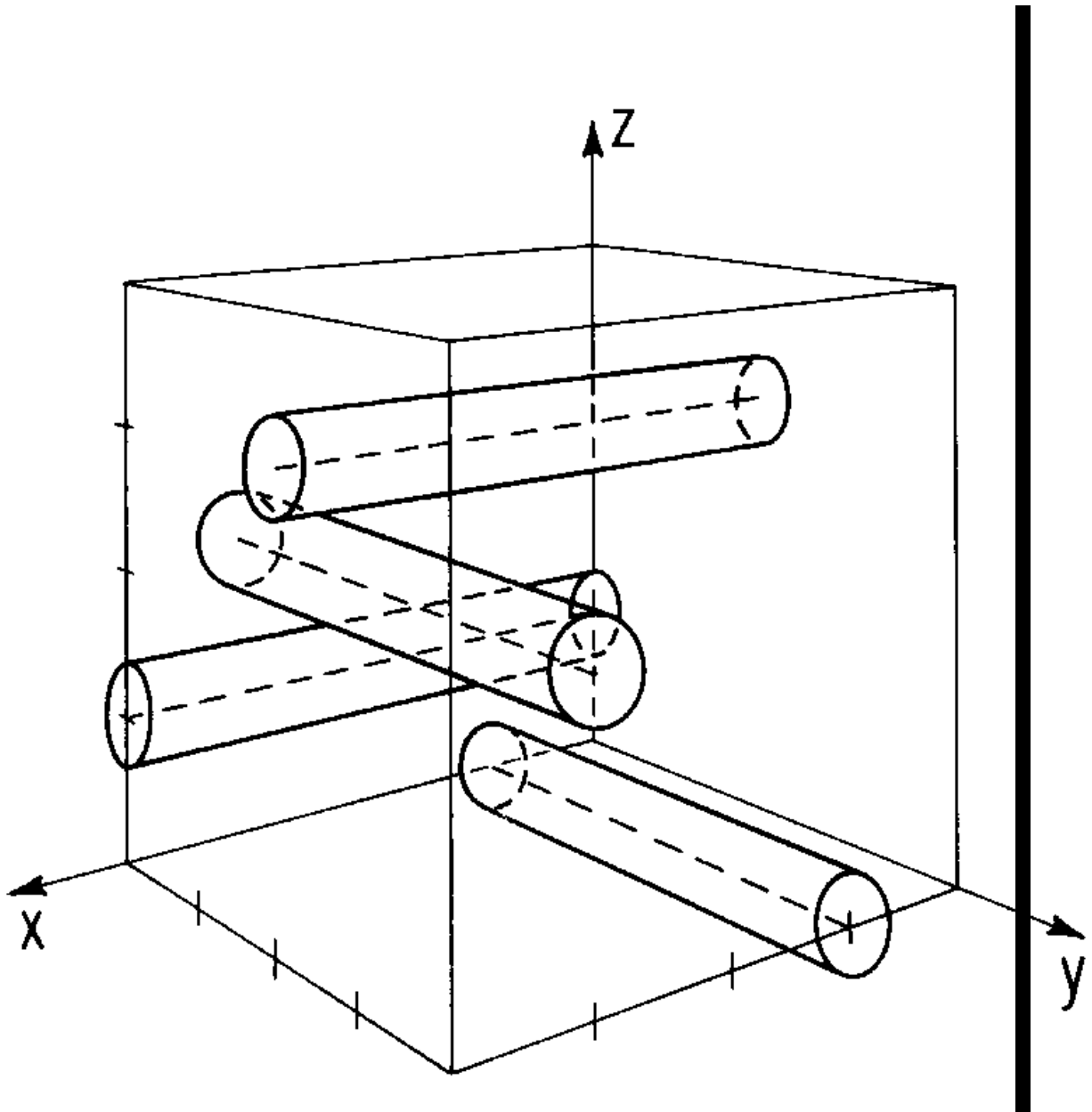


Fig. 6. Schematic representation of the lowest-order *elliptic* resonances. The dashed lines parallel to the x and y -axis represent the stable invariant lines of the $(0, 1, 0)$ and $(1, 0, 0)$ resonant surfaces respectively, which survive when $\epsilon \neq 0$ in Eq. (7). The cylinders sketch the tubular invariant surfaces that appear around these lines at finite ϵ .

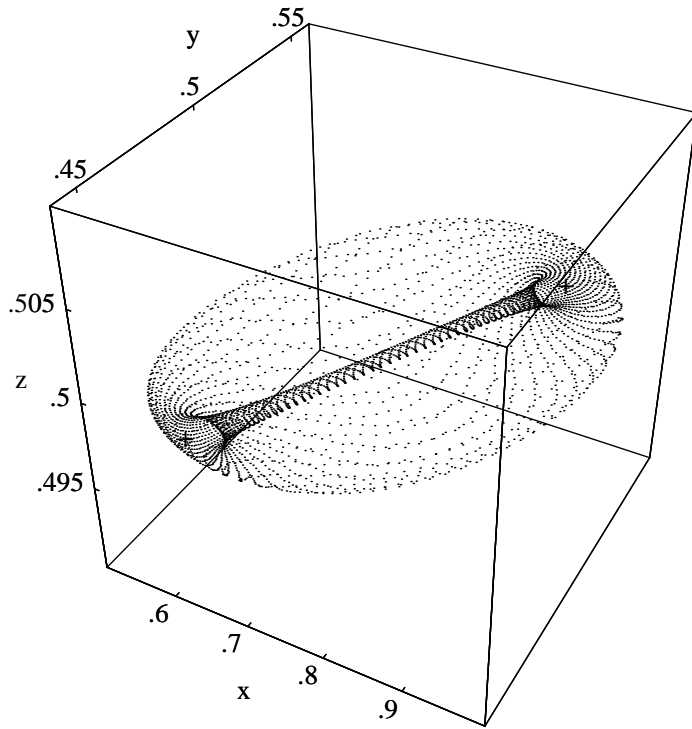


Figure 7

Fig. 7. A trajectory of (7) which lies on a toroidal invariant surface. Here, $A = 6.276$, $\alpha_B = 1$, $\alpha_C = 2$ and $\epsilon = 0.01$. The pluses denote the pair of fixed points associated with this trajectory. The coordinates are expressed in units of 2π .

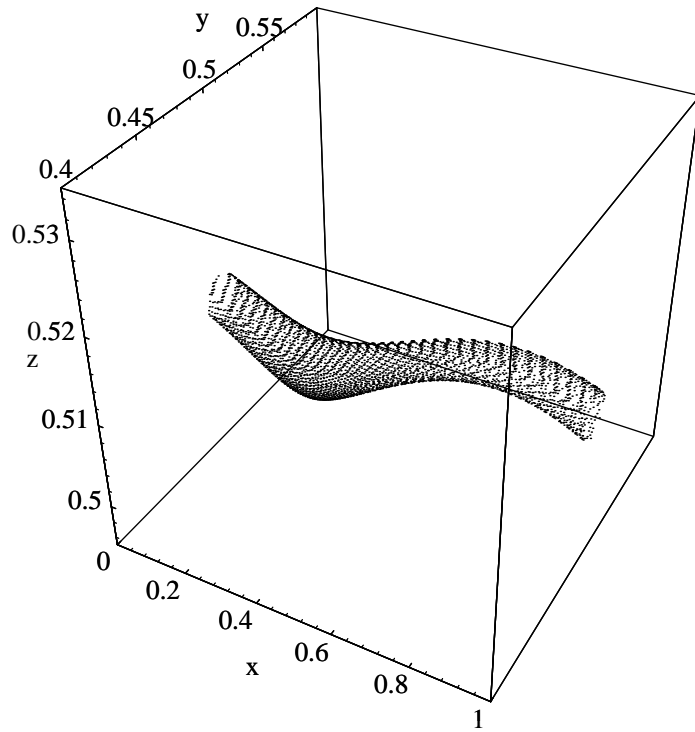


Figure 8

Fig. 8. A brand new *travelling tube* . The parameters are the same as in Fig. 7 only that $A = 6.3$. Here as well as in Fig. 7, the coordinates are expressed in units of 2π .